Si NWs based micro thermal harvesters

Bottom-up approach

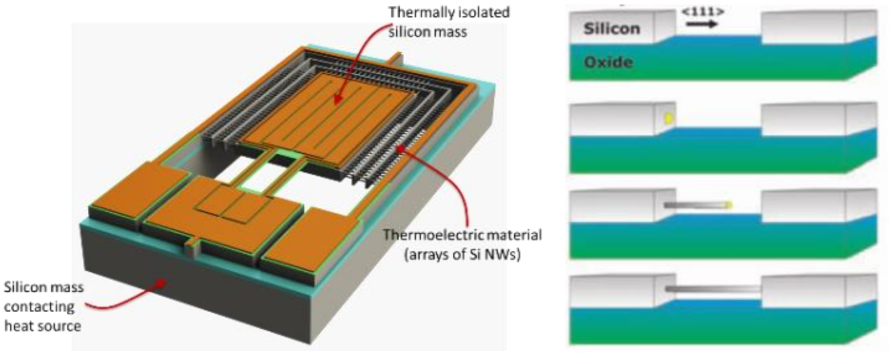

Figure 1: Left) Sketch of the bottom-up thermal harvesters, built on SOI substrates, namely a microstructure able to sustain a spatial temperature difference. Right) Bottom-up Si NWs are integrated as thermoelectric material using Au nanoparticles as seeds for the VLS method.

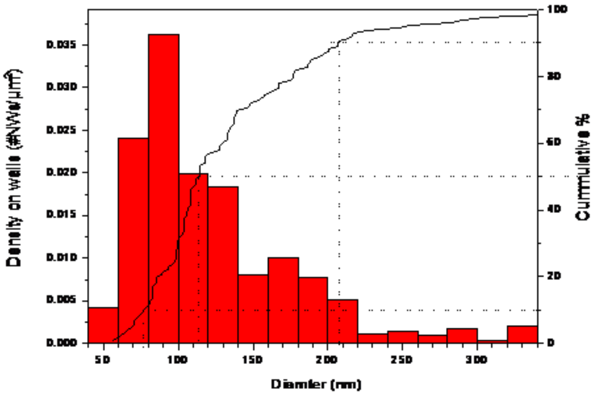

Figure 2: Diameter distribution and areal density of bottom up Si NWs grown within microplatform trenches. Cumulative count of NWs shows that mean diameter is 113nm, and 80% of NWs have diameters between 76 and 207nm.

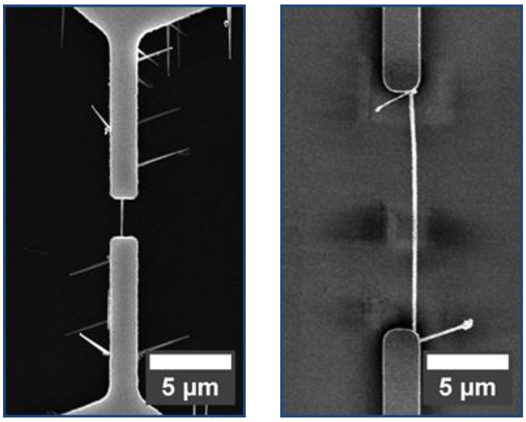

Figure 3: SEM images of test structures used in electrical and thermal conductivity measurements, which feature 15µm thick Si bars exposing <111> opposing walls that are bridged by single NWs grow from side to side during CVD growth. Si NWs in 15 and 2µm bridge, respectively

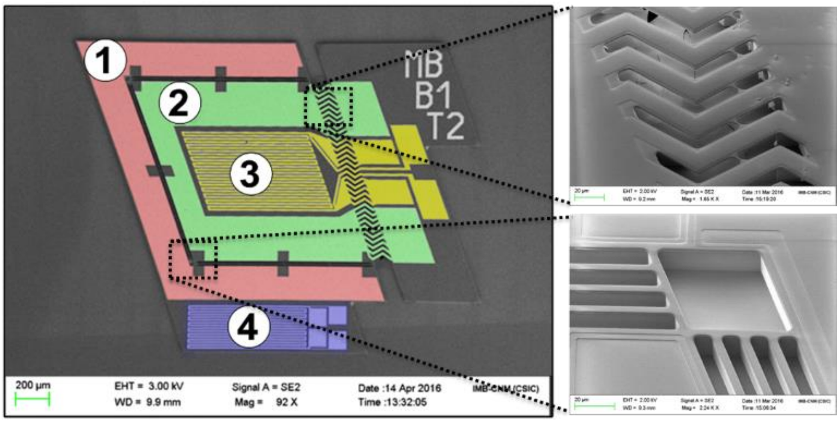

Figure 4: SEM images of actual microplatforms before Si NWs growth. Left image shows a design with 100µm long zig-zag Si_3N_4 supports. Key elements are labelled: (1) U-shaped external collector, (2) U-shaped internal collector, (3) integrated meandering heater for test purposes and (4) Si bulk temperature sensor. Right images show details of the Si_3N_4 metal supports, and a corner of the platform with four trenches. Each one has a 10µm gap and Si bars are 6µm wide.

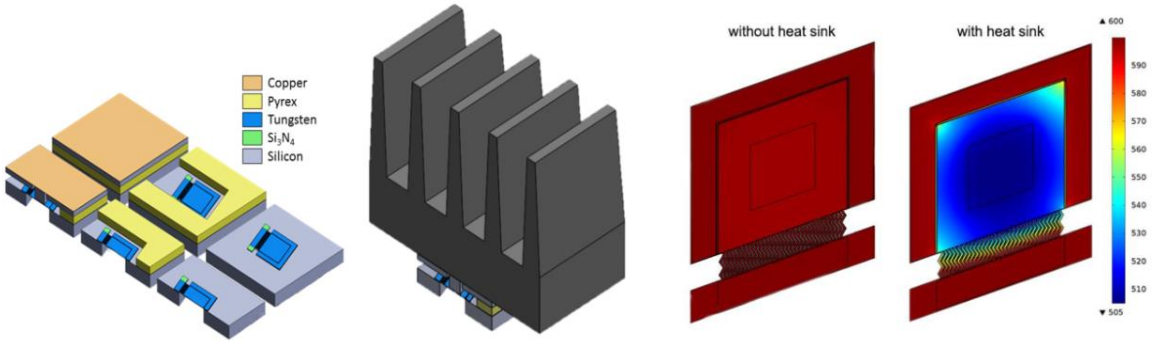

Figure 5: Left) Route devised for the heat sink integration in SiNERGY devices. A Pyrex spacer is used to place a silicon adapter on top of device, with a silicon column to properly contact suspended platform and a top copper film as interface with the metallic heat sink. Right) Temperature distribution with and without the heat sink obtained from FEM simulations. Device bottom temperature is fixed at 600K and top surface has a natural convection to an ambient temperature of 300K. Temperature span without a heat sink is only 3K, while with the heat sink it reaches almost 100K.

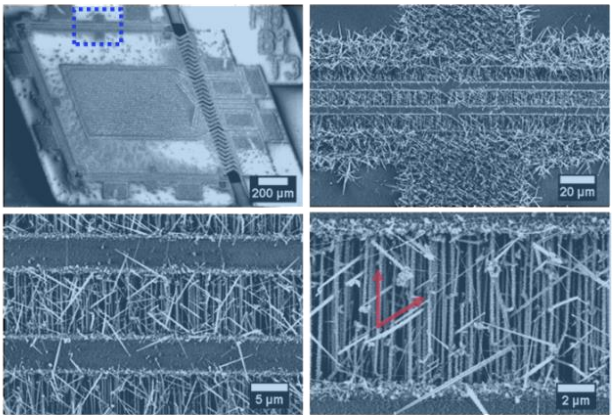

Figure 6: False-color SEM images of Si NWs grown in a mircoplatform with four trenches, with details of the NWs inside one of the 10µm gap

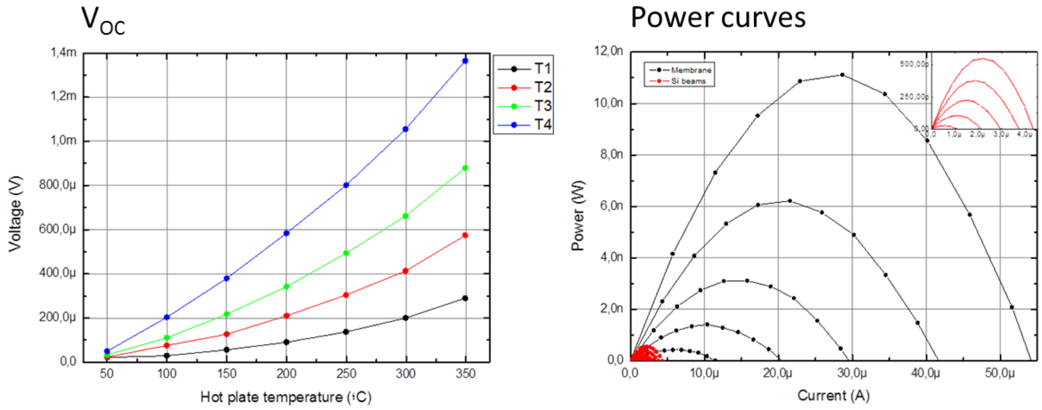

Figure 7: Left) Thermovoltage obtained with SiNERGY devices placed on a hot surface. Impact of the NWs effective length (1 to 4 trenches). Right) Power curves for devices with three NWs trenches using SiNERGY optimized platforms (dotted line) or a previous design with Si beams (detailed in the inset). Curves were obtained at different temperatures (50 to 300°C, in 50°C steps).

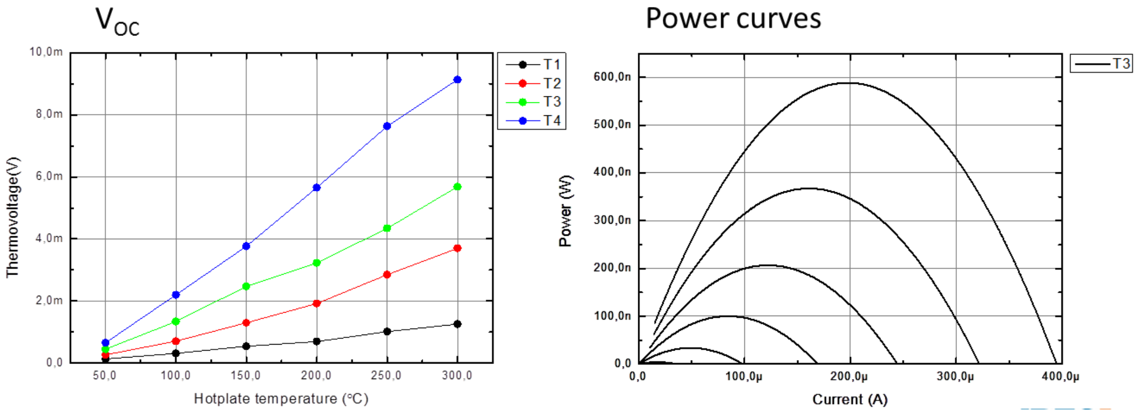

Figure 8: Left) Thermovoltage generated by SiNERGY devices placed on a hot surface when using force convection to emulate the effect of a heat sink. Voltage increases by a factor 8 with respect to the still air case. Right) Power curves

Top-down approach

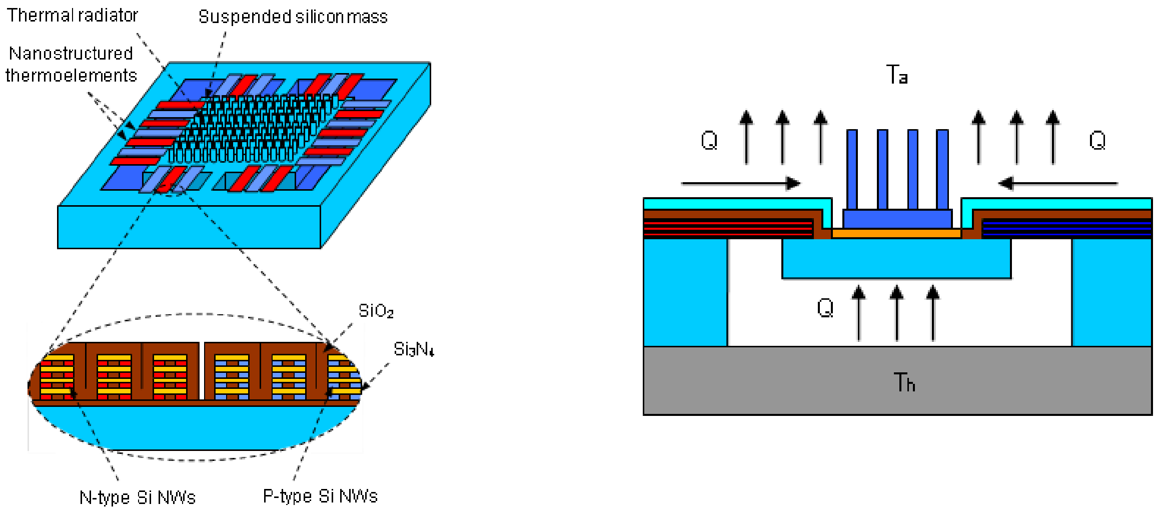

Figure 9: Prospective and side view of the top-down TEG

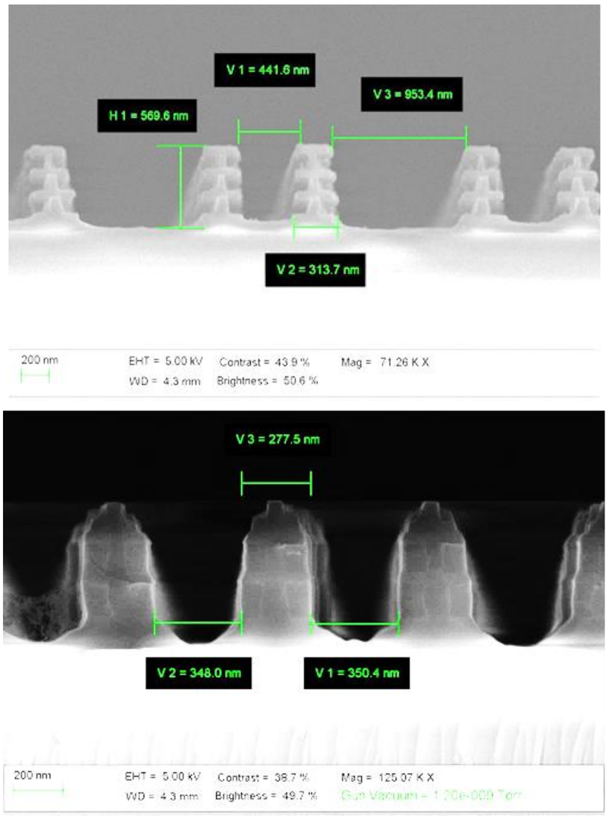

Figure 10: SEM micrographs of the mold (top) and of the grown encapsulated SiNWs

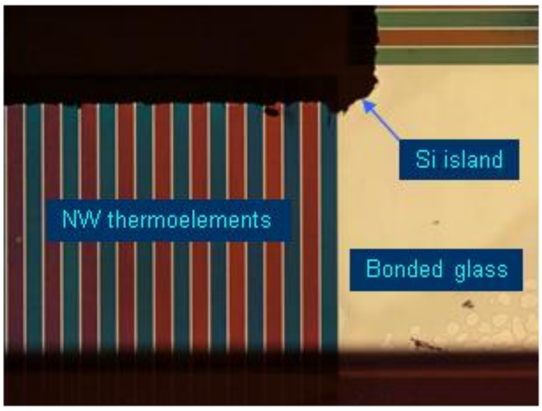

Figure 11: Details of a test structure

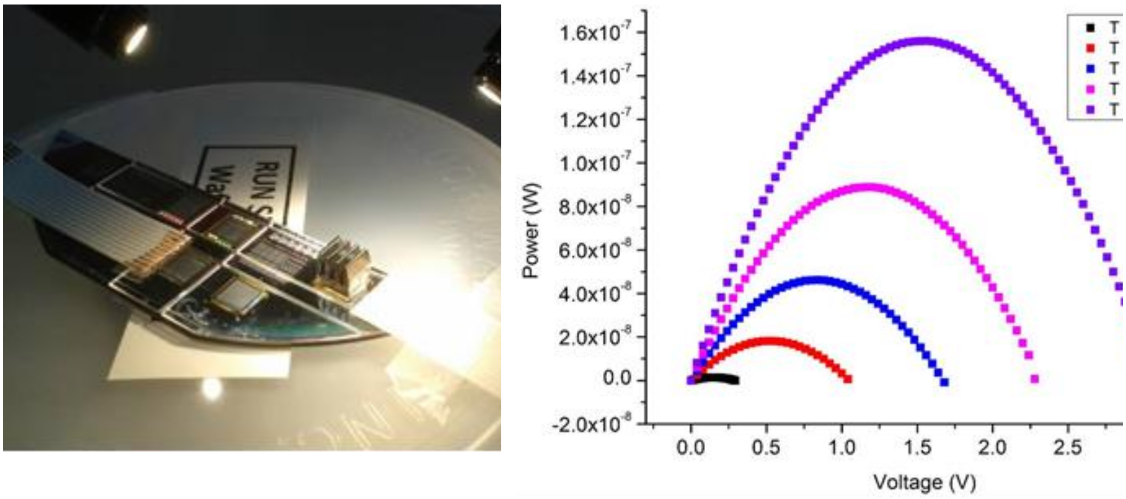

Figure 12: (left) Thermovoltage measurement setup and (right) Power voltage characteristics of the top-downTEG in response to variations of the applied temperature difference.

Mechanical energy harvesters

Electrostatic approach

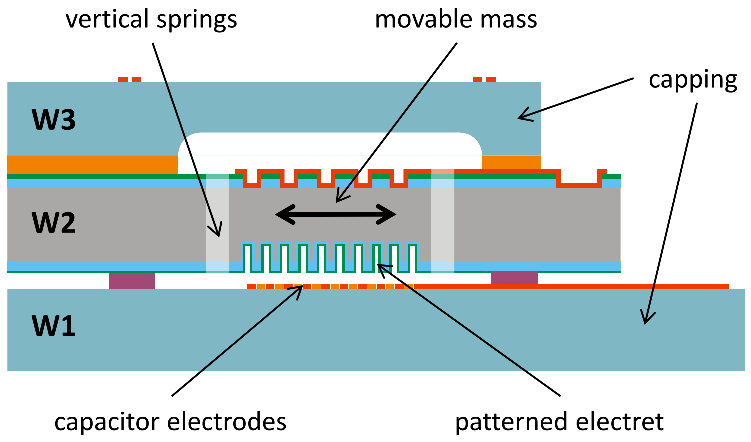

Figure 13: schematic cross-section of the 1st generation electrostatic energy harvester, showing the key components of the device.

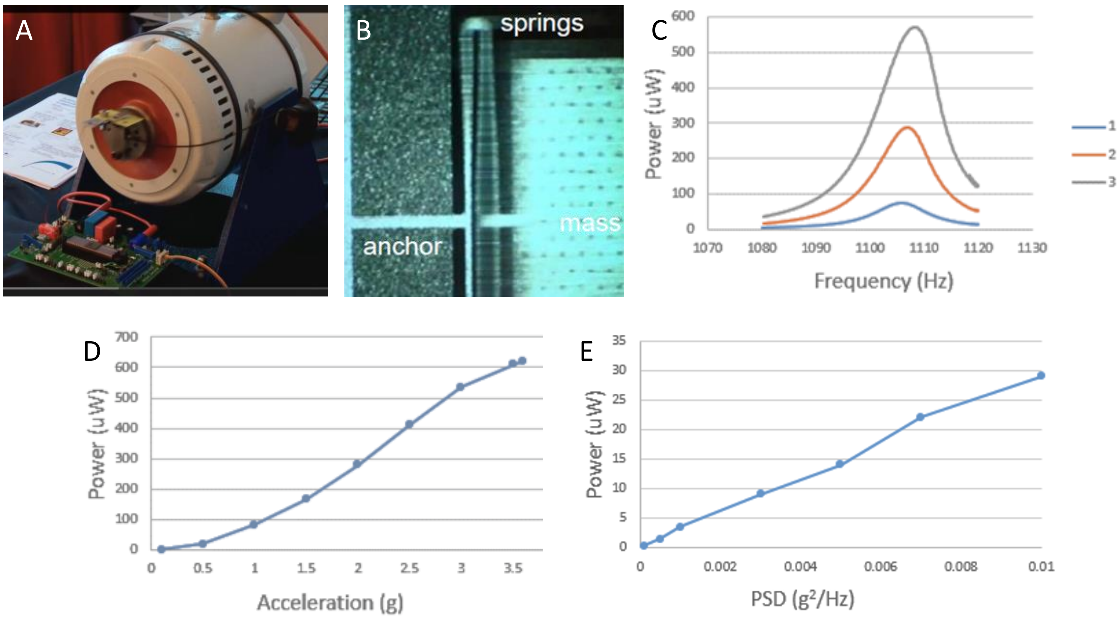

Figure 14: A) shaker setup with harvester; B) visualization of mass movement; C) resonance curves for different input accelerations; D) output power as function of sinusoidal input acceleration; E) output power as function of white noise input

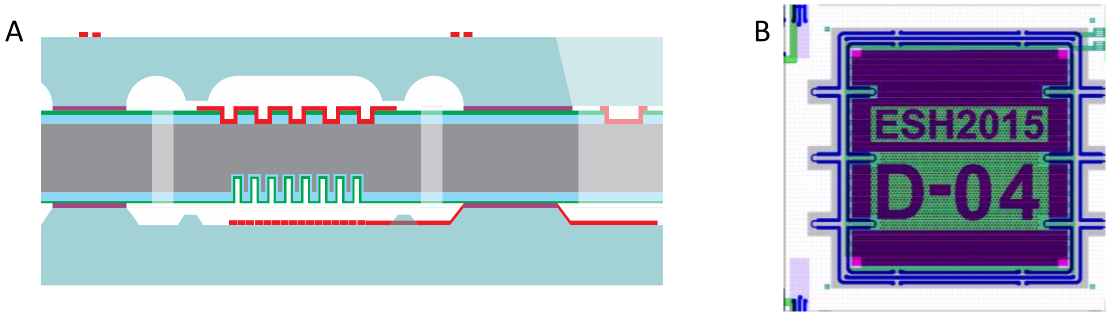

Figure 15: A) schematic cross-section of the 2nd generation electrostatic harvester with thin SU-8 bond and cavities with dimples and B) top view mask layout showing the 6 long flexible Si bumpers

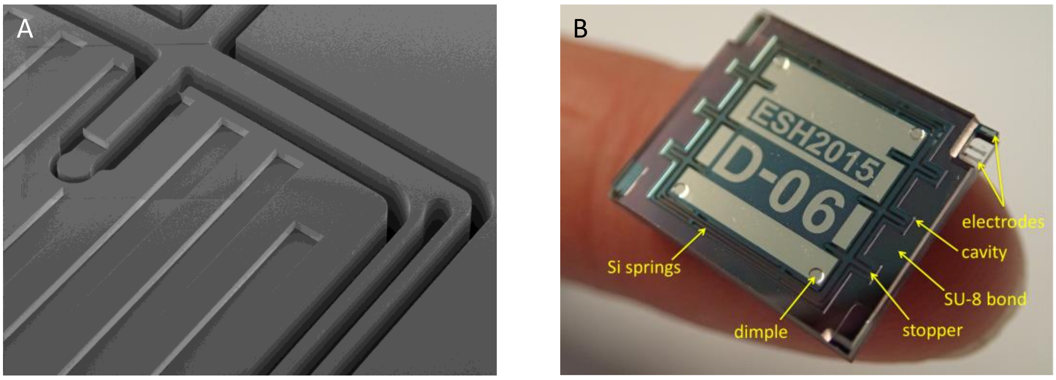

Figure 16: A) SEM picture showing the DRIE etched springs, flexible stopper and electret lines; B) finalized 2nd generation electrostatic energy harvester

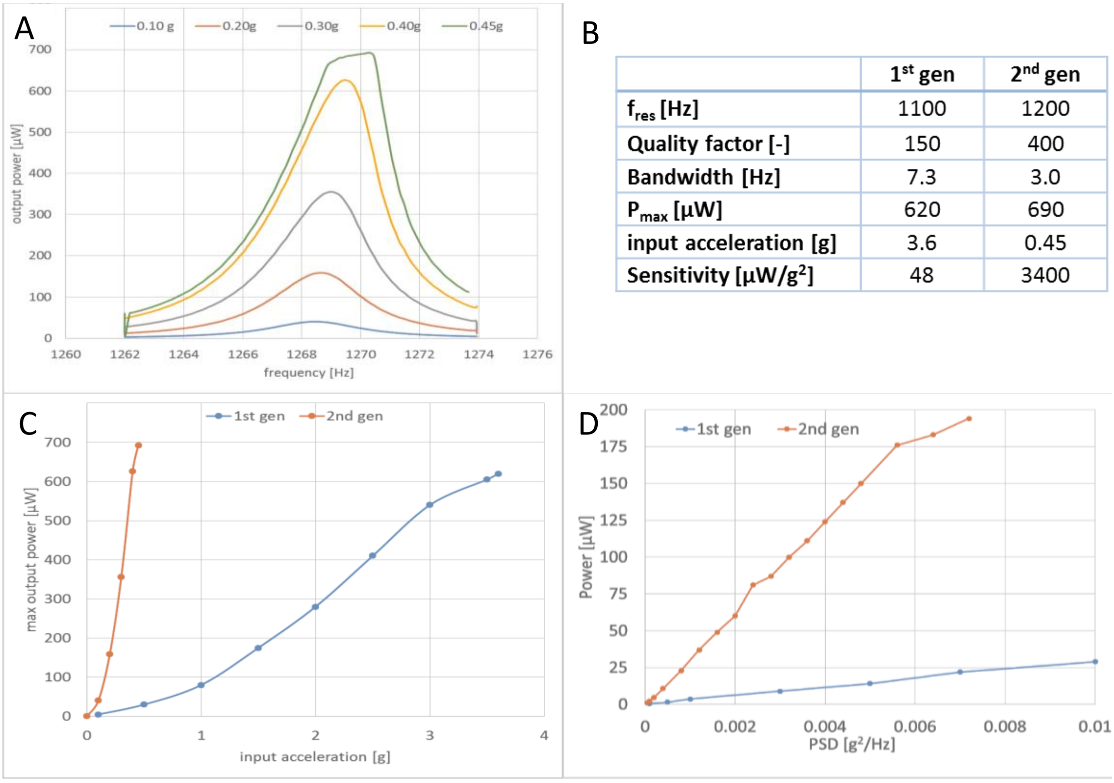

	1^{st} gen	2^{nd} gen
f_{res} [Hz]	1100	1200
Quality factor [-]	150	400
Bandwidth [Hz]	7.3	3.0
P_{max} [µW]	620	690
input acceleration [g]	3.6	0.45
Sensitivity [µW/g^2]	48	3400

Figure 17: A) resonance curves for different input accelerations; B) table with mechanical characteristics of the 1st and 2nd generation devices; Output power as function of the sinusoidal (C) and noise (D) input acceleration, showing the very high sensitivity of the 2nd generation devices

Piezoelectric approach

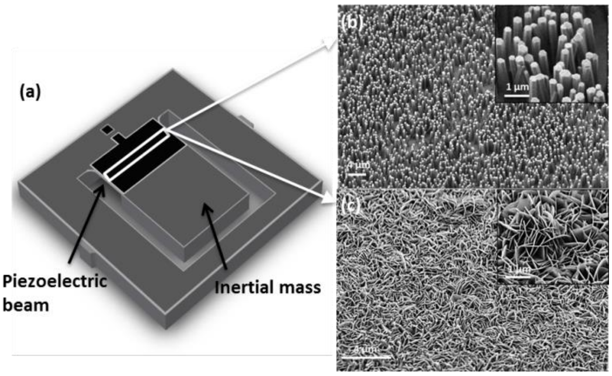

Figure 18: Functional device configuration. (a) A cantilever structure for mechanical out-of-plane motions, with the two different ZnO nanostructures for piezoelectric transduction: nanosheets (b) and nanowires (c)

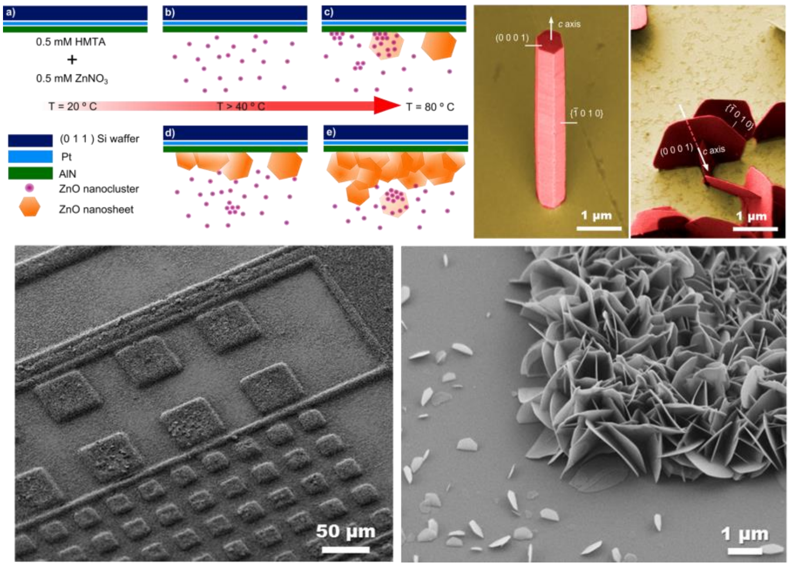

Figure 19: Hydrothermal growth of ZnO nanosheets (a). Comparison between nanowire an nanosheet orientation (b) and patterning of areas where nanosheets have been grown (c and d).

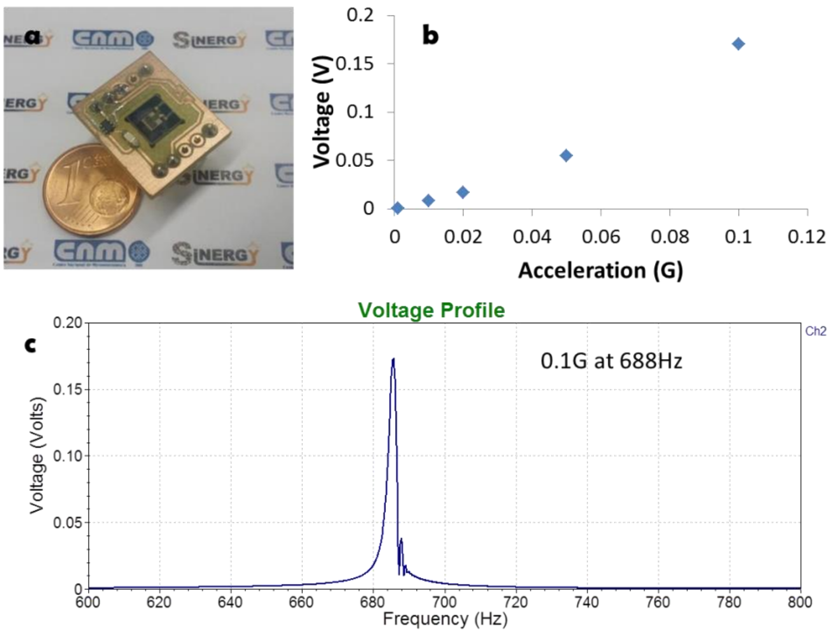

Figure 20: Image of AlN-based device mounted on ad-hoc PCB (a), dependence of generated open-circuit voltage with input acceleration value (b) and frequency response with a load resistance of 1 MΩ at 0.1 g to find the resonance frequency at 688 Hz (c)

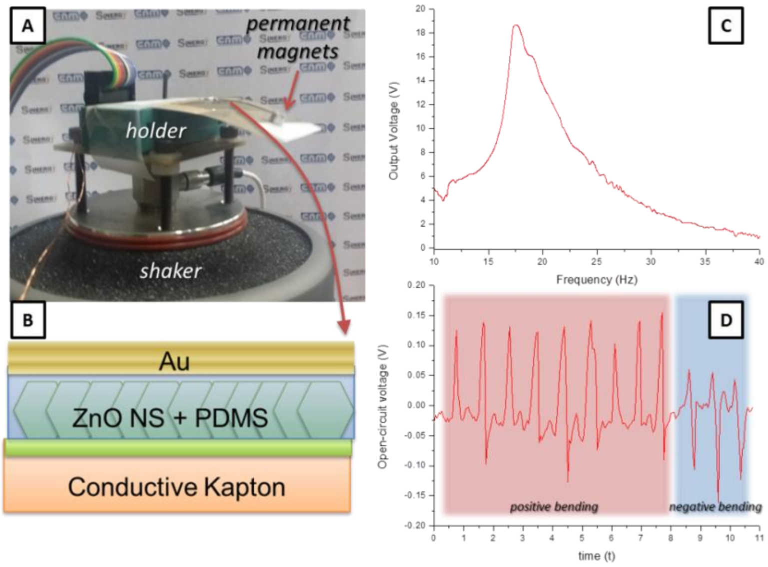

Figure 21: Flexible device mounted on top of an electromagnetic shaker to be tested at a controlled vibration at a certain frequency and acceleration (a), cross section showing the materials used in the thin film (b), output voltage generated by the test device showing a resonance peak at 17.5Hz for an acceleration of 0.5 g (c) and open-circuit voltage generated by the test device when applying a positive and negative bending to the film (d)

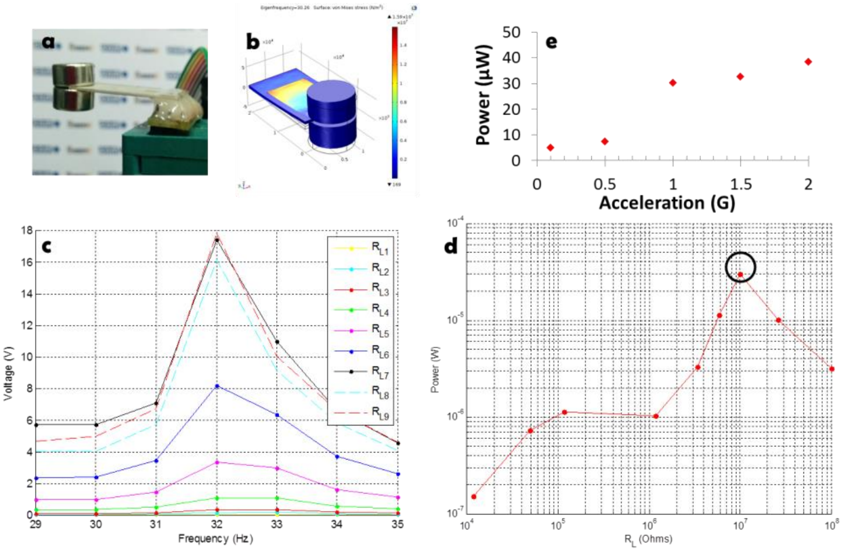

Figure 22: Image of fabricated 1st generation prototype (a), FEM simulations used to optimize the generator (b), voltage generated by the device vs. vibration frequency (c), extracted power vs. load resistance (d) and generated power versus acceleration magnitude (e).

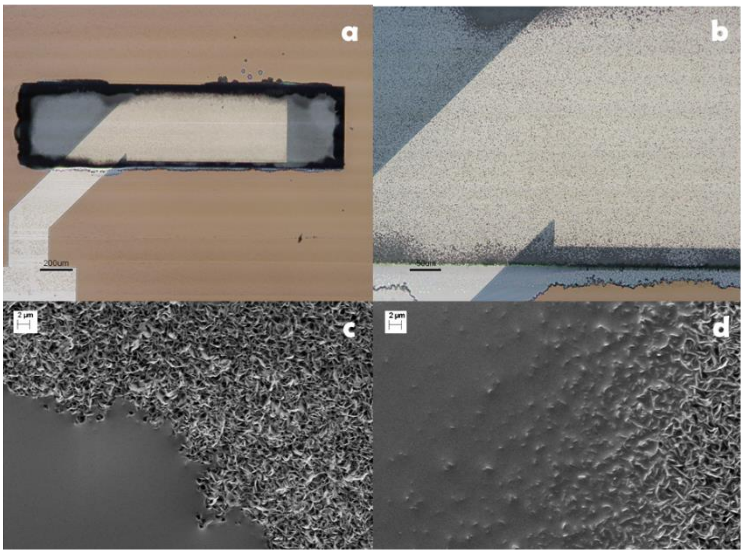

Figure 23: Optical image of ZnO NSs embedded by inkjet-printed SU8 on top of a device bottom electrode and higher magnification image showing detail of different layer edges (b). SEM images of ZnO NSs partly covered by inkjet-printed SU8 to validate the successful SU8 percolation (c and d).

Thin film solid state batteries

LiMn2O4 based battery

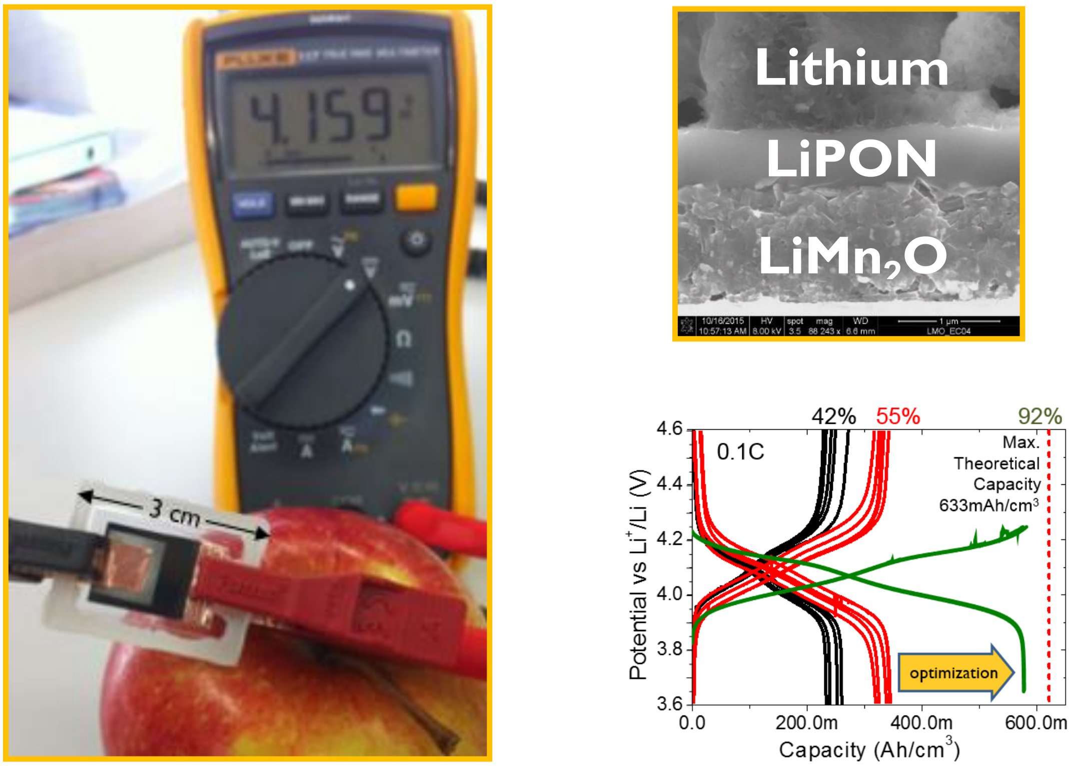

Figure 24: a) Battery stack glass encapsulation. b) Cross section SEM of a full battery stack of ***LMO/LiPON/Lithium*** *c) Charge/Discharge measurement and optimization of battery stack.*

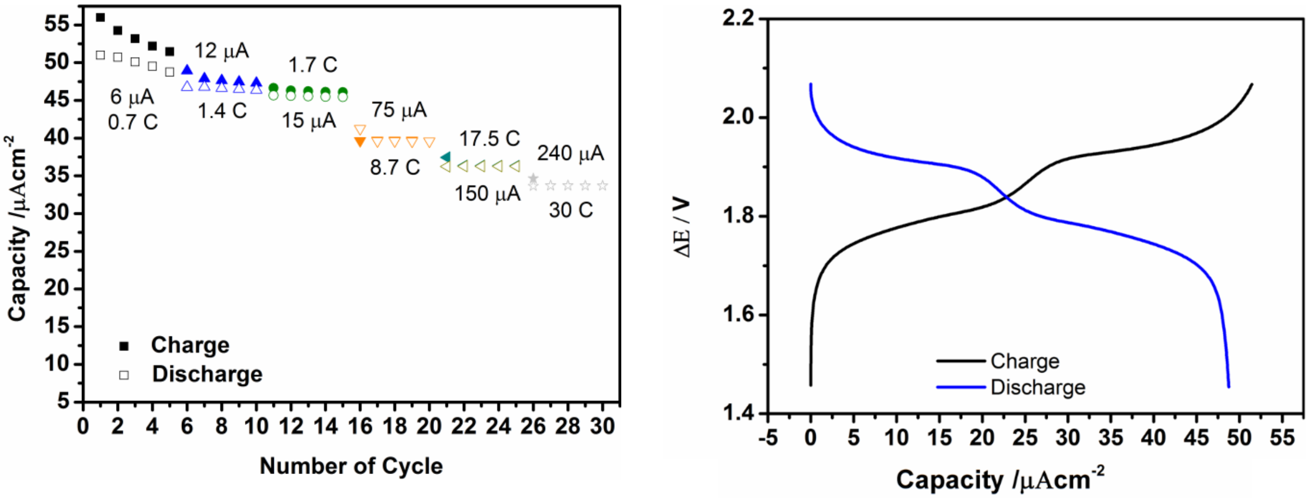

Figure 25: Rate capability under different current rates and Charge/discharge cycle at 15µA of a full battery based on ***LMO/Li_2SO_4:$ZnSO_4$/Zinc***

Li4Ti5O12 based battery

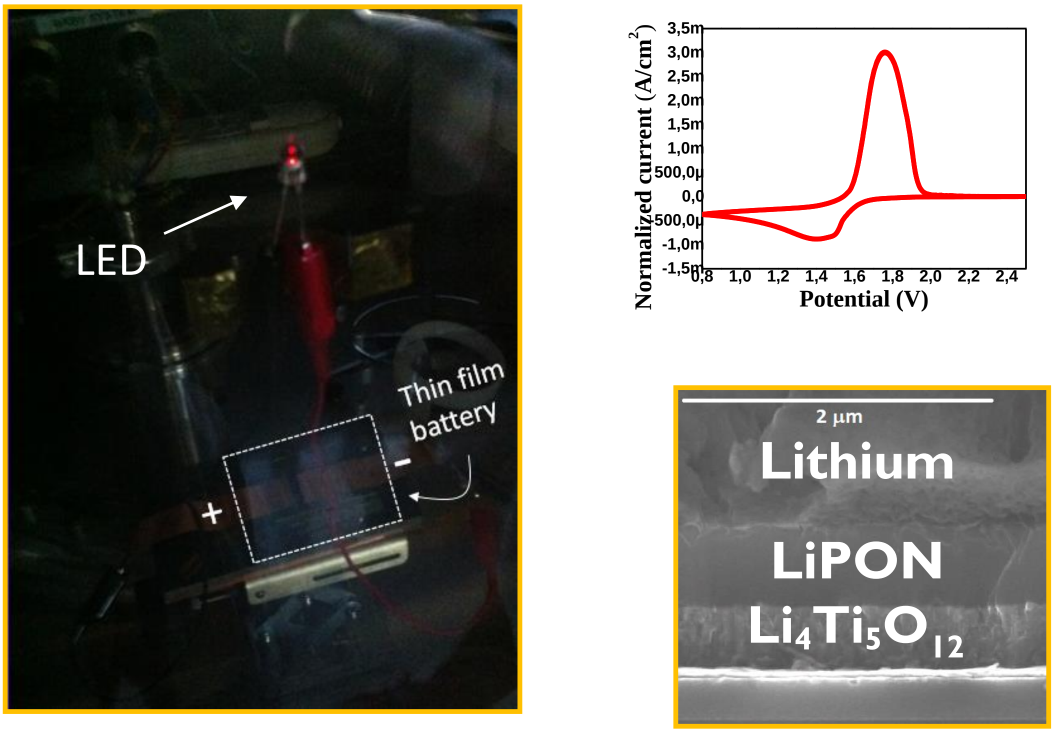

*Figure 26: a) Full battery stack **LTO/LiPON/Lithium** able to light an LED for several minutes. b) Cyclic voltammogram of the battery stack. c) Cross section SEM of battery stack*

3D thin film battery proof of concept

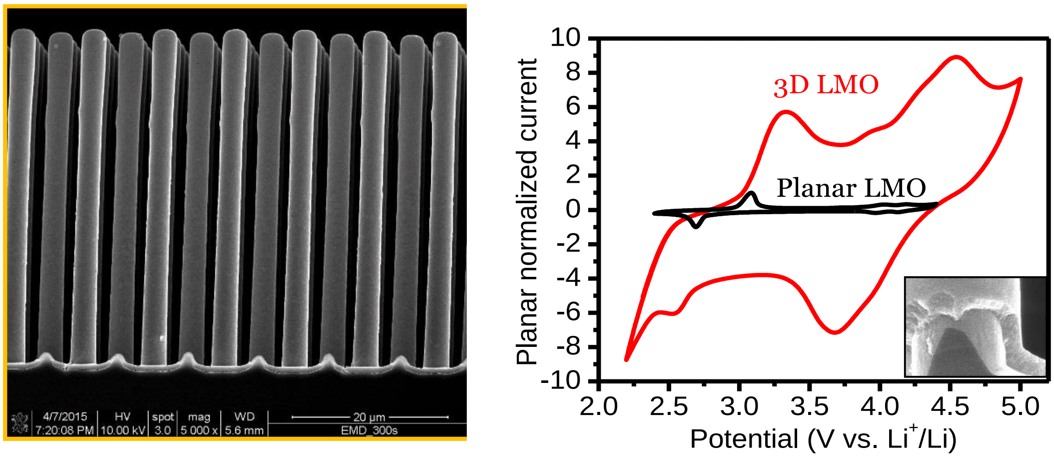

Figure 27: SEM image (cross section) of a 350nm MnO2 film grown by ECD on 3D pillar structures b) Cyclic voltammogram of a 3D electrode compared to a planar electrode.

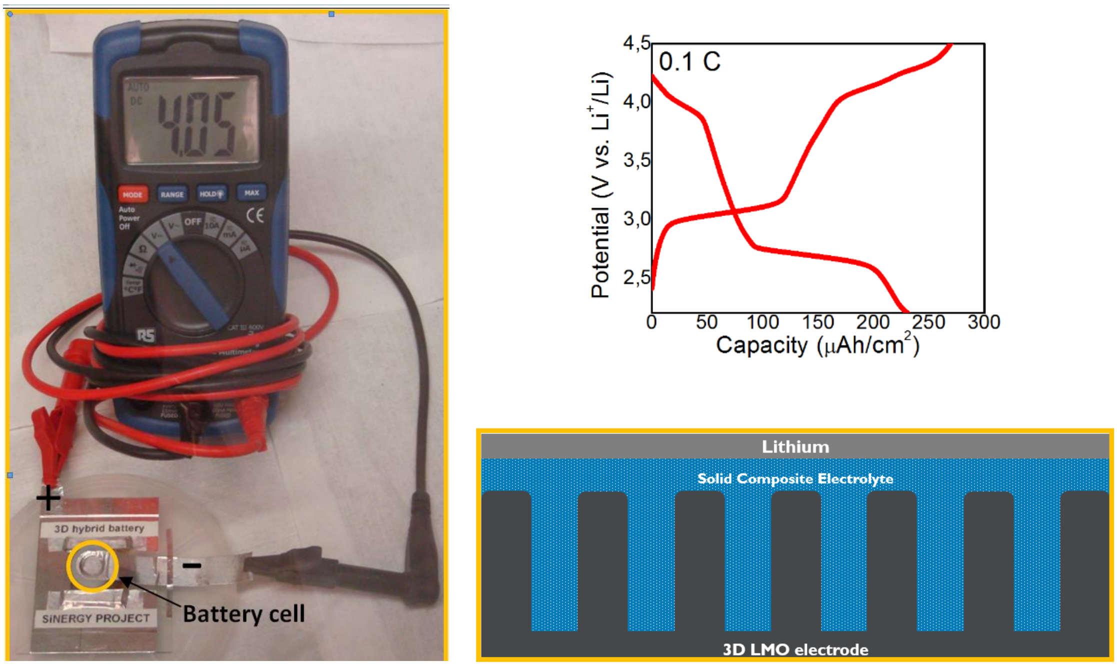

Figure 28: a) 3D hybrid battery ***LMO/SCE/Li*** *showing a stable potential around 4 V. b) Charge/Discharge measurement at 0.1 C of the 3D battery. C) Schematic representing the different layers in the stack.*

Feasibility integration in application scenarios

Fully autonomous tire pressure monitoring system (TPMS) demonstrator

Figure 29: TPMS module transfer from valve mounted towards tire integration

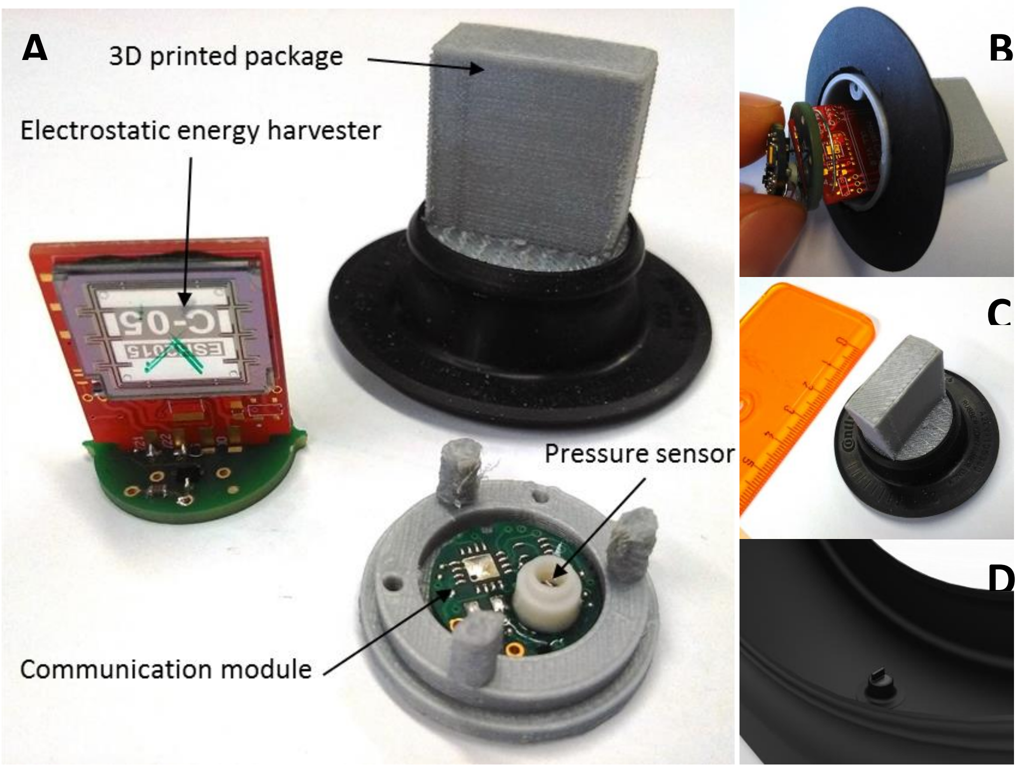

Figure 30: A) Components of the TPMS patch, consisting of PCB board with electrostatic energy harvester and direct charge PM, board with communication module and sensors and 3D printed package. B) PCB boards inserted in TPMS patch. C) size indication of the TPMS patch. D) impression of new TPMS demonstrator mounted inside tire

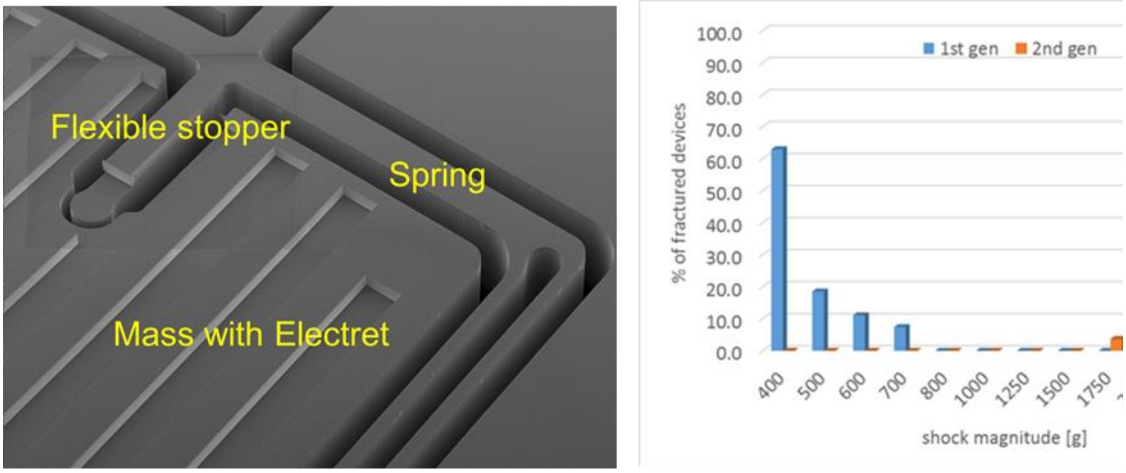

Figure 31: (left) SEM picture of electrostatic energy harvester with flexible silicon stopper of 2nd generation device. (right) drop tester results showing improvement for 2nd generation device.

Thermal electric generator (TEG) demonstrator

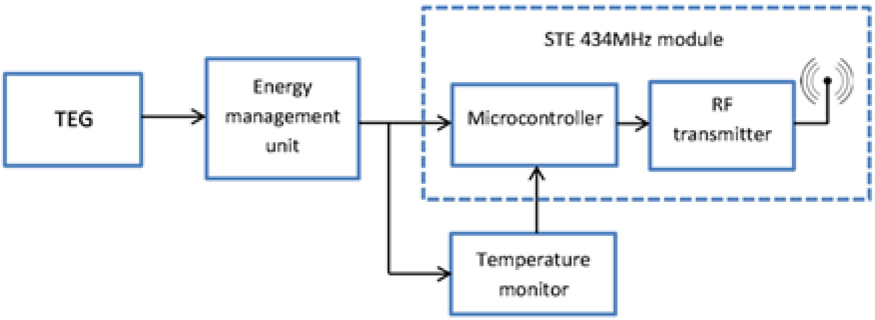

Figure 32: Block diagram showing the system design for the autonomous wireless temperature sensor for the gas powered fryer

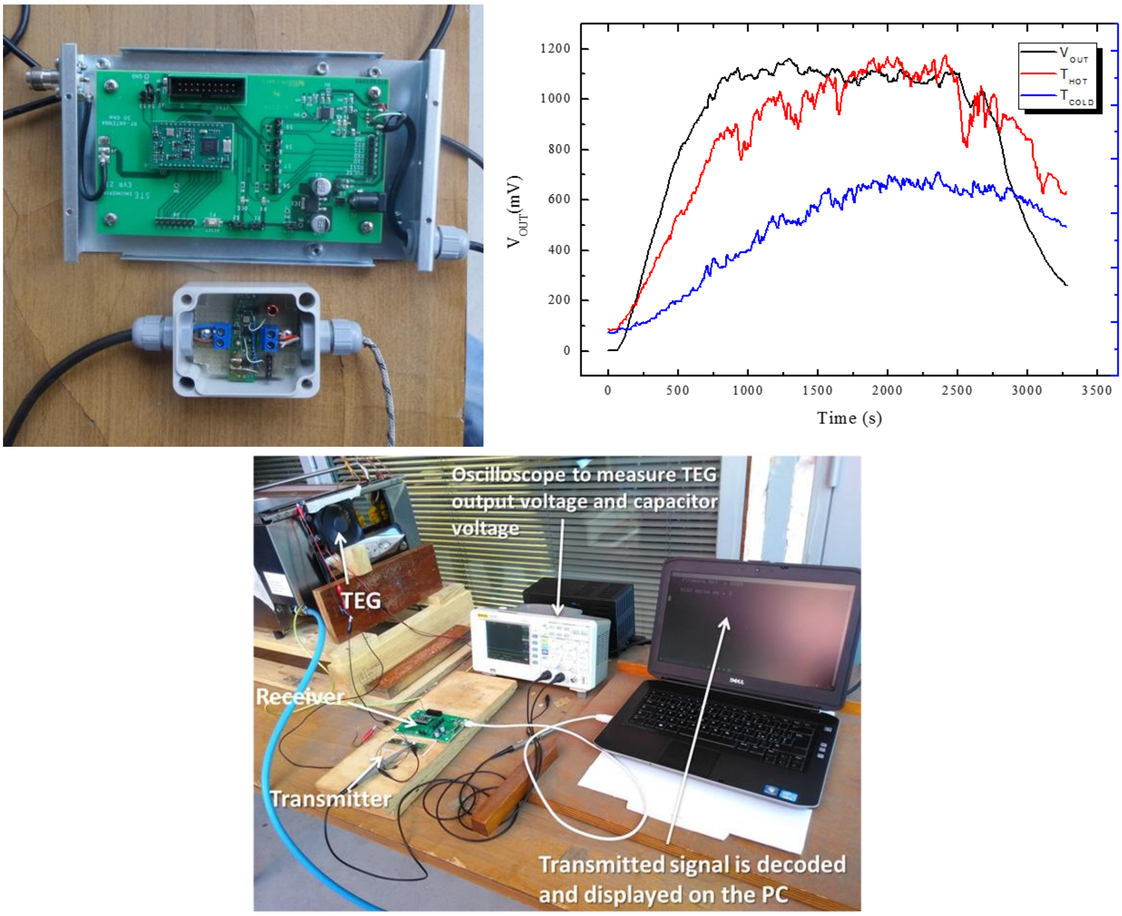

Figure 33: Thermal harvester setup: (top left) Details of the RF receiver and of the power management unit: (top, right) Thermovoltage measured under operative conditions; (bottom) overview of the system.

Piezoelectric energy harvester (PEH) demonstrator

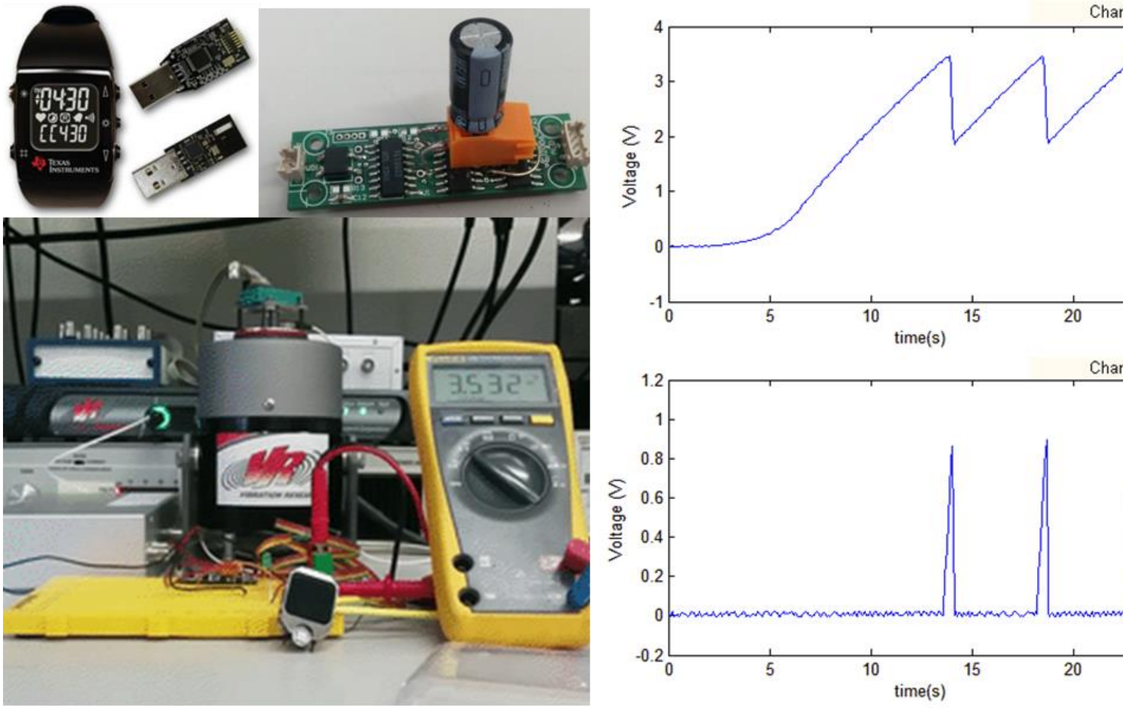

Figure 34: EZ430 kit and EH300 kits used for the PEH demonstrator. Characterization setup of PEH demonstrator. Output voltage generated by the energy harvester and current pulses generated when the application circuit is powered.